

Article

# Characterization of Polyethylene Oxide and Sodium Alginate for Oil Contaminated-Sand Remediation

Jongwon Jung<sup>1</sup> and Jong Wan Hu<sup>2,3,\*</sup>

<sup>1</sup> Department of Civil and Environmental Engineering, Louisiana State University, Baton Rouge, LA 70803, USA; jjung@lsu.edu

<sup>2</sup> Department of Civil and Environmental Engineering, Incheon National University, Incheon 22012, Korea

<sup>3</sup> Incheon Disaster Prevention Research Centre, Incheon National University, Incheon 22012, Korea

\* Correspondence: jongp24@incheon.ac.kr; Tel.: +82-32-835-8463; Fax: +82-32-835-0775

Academic Editor: Marc Rosen

Received: 27 September 2016; Accepted: 27 December 2016; Published: 4 January 2017

**Abstract:** Biopolymers have been employed in many soil applications, such as oil-contaminated soil remediation, due to their environmentally friendly characteristics. This study focused on changes in the wettability and viscosity of polyethylene oxide (PEO) and sodium alginate (SA), according to the variation in concentration and their impact on oil-contaminated soil remediation using biopolymer-decane displacement tests. The contact angle and interfacial tension vary with concentration by adding biopolymer to water; however both parameters yield relatively constant values within the range of 2–10 g/L for the concentration of PEO and SA. In this study, their influence on fluid invasion patterns is insignificant compared to viscosity and flow rate. Viscosity increases with the concentration of PEO and SA, within the range of 0–10 g/L, which causes the biopolymer-decane displacement ratio to increase with concentration. Biopolymer-decane displacement increases with injected fluid velocity. At low flow rates, the effect of the biopolymer concentration on the displacement ratio is prominent. However the effect decreases with an increase in flow rate. Thus both biopolymer concentration and injection velocity should be considered to achieve the economic efficiency of soil remediation. The experimental results for the distribution of soils with different grain sizes indicate that the displacement ratio increases with the uniformity of the coefficient of soils.

**Keywords:** remediation; polyethylene oxide; alginic acid sodium salt

## 1. Introduction

To improve the soil properties, organic agents such as polymers, biopolymers and surfactants have been developed, which indicate their capability of improving the shear strength and stiffness of soil [1–8]. Biopolymers, such as polyacrylamide (PAM), have demonstrated their effect on irrigation by increased water infiltration and decreased erosion due to their water-absorbing capacity [9–13]. Biopolymers have been employed in enhanced oil recovery (EOR) due to their high viscosity and effect on the water-flood performance in EOR [14–16]. Thus the oil-flooding tests performed in the laboratory and the field using biopolymers have demonstrated the efficiency of biopolymers and polymers in EOR [17–19]. Considering their high viscosity and properties, biopolymers have been considered for oil-contaminated soil remediation at shallow depths [20–22]. Biopolymers are environmentally friendly materials that are produced from an ecosystem and are distinguished from polymers. For example, polyethylene oxide (PEO) can be produced by the interaction of ethylene oxide with water, ethylene glycol, or ethylene glycol oligomers [23], and sodium alginate (SA) is a natural polysaccharide product that is extracted from brown seaweeds, which grow in cold-water regions [24]. Thus they do not influence geo-environments after their use. Recently the characteristics of water-soluble polymers, including contact angle, interfacial tension, and viscosity, have been explored for the better utilisation

of biopolymers in soil remediation and EOR [7,8]. Cao et al. (2016) presented the characteristics of biopolymers, such as chitosan, PEO, xanthan gum, SA, and polyacrylic acid, in order to use them for soil remediation [8]. However the completed testing was conducted with one or two concentrations of each biopolymer [8]. Thus the selection of the injection conditions of biopolymers into oil-contaminated soil, such as the concentration of biopolymer and the injection rate, is difficult. The engineering behaviours of biopolymers have been investigated using two-dimensional micromodels [8], which have the limitation of simulating three-dimensional field conditions. Thus the physical properties of biopolymers within an extensive range of biopolymer concentration (i.e., 0, 2, 5 and 10 g/L) was investigated, and the flow of biopolymer solutions using three-dimensional column tests was identified in this study.

## 2. Previous Studies

### 2.1. Biopolymer in Soil Remediation and Enhanced Oil Recovery

Soil contamination at industrial sites caused by mining heaps, dumping, natural settlement, and quarries has increased [25]. To reduce soil contamination, several soil remediation techniques that include excavation, soil vapour extraction, bioremediation, surfactant-enhanced remediation, and steam injection have been developed [26–30]. Soil excavation benefits from technical efficiency but is costly and limited for landfill sites [27]. Thus soil vapour extraction, surfactant-enhanced remediation, and steam injection have focused on soil remediation [31]. Biosurfactants, which are surface-active substances that are synthesised by cells, have been employed for oil-contaminated soil remediation due to their low surface tension [32,33]. Biopolymers are environmentally friendly materials as they are synthesised from plants [34]. Thus biopolymers have been investigated to improve the mechanical properties of sand [34]. Previous studies have proven the effect of biopolymers on improvements in the mechanical properties of soils [35,36]. Recently biopolymers have been explored for oil-contaminated soil remediation, instead of biosurfactants [8]. The results indicate that the majority of biopolymers, such as PAM, chitosan (85% deacetylated power), PEO, xanthan gum (xanthan), SA, and polyacrylic acid (PAA), have high viscosity and cause the oil-biopolymer solution displacement to increase in micromodel tests [8]. Water flushing, including soluble biopolymers, has been employed to enhance oil recovery due to their high viscosity and have been applied in the remediation of petroleum waste-contaminated sites [37–43]. The high viscosity of biopolymers causes an increase in both capillary number and mobility of fluid (Equations (1) and (2)). Capillary number is dependent on fluid velocity, fluid viscosity, and surface tension. Mobility is a relative measurement of how easily a fluid moves through porous media, which is defined as the ratio of the effective permeability to the fluid viscosity [44].

### 2.2. Polyethylene Oxide

PEO can be produced by the interaction of ethylene oxide with water, ethylene glycol, or ethylene glycol oligomer [23], which is a synthetic polyether with high-molecular-weight polymers (Figure 1a). PEO is amphiphilic and soluble in water and various organic solvents. PEO has been employed in pharmaceutical products, such as lubricating eye drops, and as a viscosity modifier for polymer flooding in EOR due to its high viscosity [14–16]. PEO, which is a nonionic surfactant, has been considered to be the most favourable material for soil remediation due to its intermediate sorption and low biotoxicity [45].

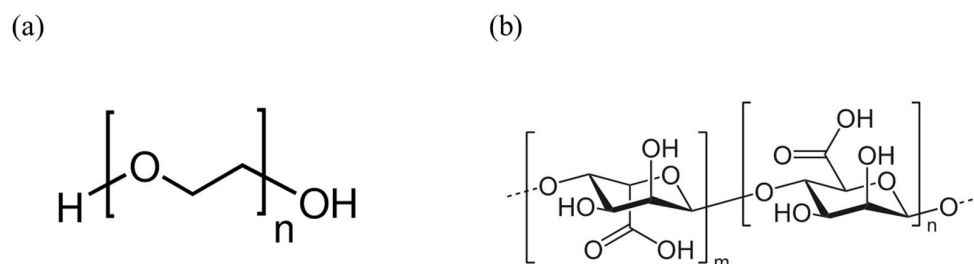


**Figure 1.** Chemical composition structure of (a) polyethylene oxide (PEO) and (b) sodium alginate (SA).

### 2.3. Sodium Alginate

SA is a natural polysaccharide product that is extracted from brown seaweeds, which grow in cold-water regions (Figure 1b) [24]. SA becomes soluble in cold and hot water with strong agitation and can be thick and bound together. SA has been employed in the food industry as an emulsifier to increase the viscosity. SA has been employed to form impervious barriers in silty soil with a maximum increase in shear strength of 50% [24].

## 3. Experimental Methods

### 3.1. Materials

Commercial PEO (Acros organics, Geel, Belgium) and SA (MP Blomedicals, Santa Ana, CA, USA) were selected in this study. The chemical structures of PEO and SA are presented in Figure 1. Various biopolymer concentrations (i.e., 0, 2, 5, and 10 g/L) were prepared by dissolving the prescribed mass of polymer powders into a 1000 mL volumetric flask; the mixtures were mechanically stirred (Isotemp Stirring Hotplate 4 × 4 in. model, Fisher Scientific) for 24 h. Decane (Sigma-Aldrich, St. Louis, MO, USA, anhydrous, >99%,  $\text{C}_{10}\text{H}_{22}$ ) was employed to simulate the oil in oil-contaminated soils. Decane is a constituent of petroleum [46–54] and represents the petroleum contaminant in soils due to its interfacial properties, which affect fluid flow patterns in porous media [52–54]. Ottawa sands that have different particle size distributions were employed in this study (Figure 2). Table 1 lists the effective size of the sands ( $D_{10}$ ), the coefficient of uniformity ( $C_u = D_{60}/D_{10}$ ), and the coefficient of gradation ( $C_c = D_{30}^2/(D_{60} \times D_{10})$ ), where  $D_{10}$ ,  $D_{30}$ , and  $D_{60}$  denote the grain diameters at 10% passing, 30% passing, and 60% passing, respectively. Both samples are poorly graded but Figure 1 shows the distinct difference in the particle size variation of both samples.

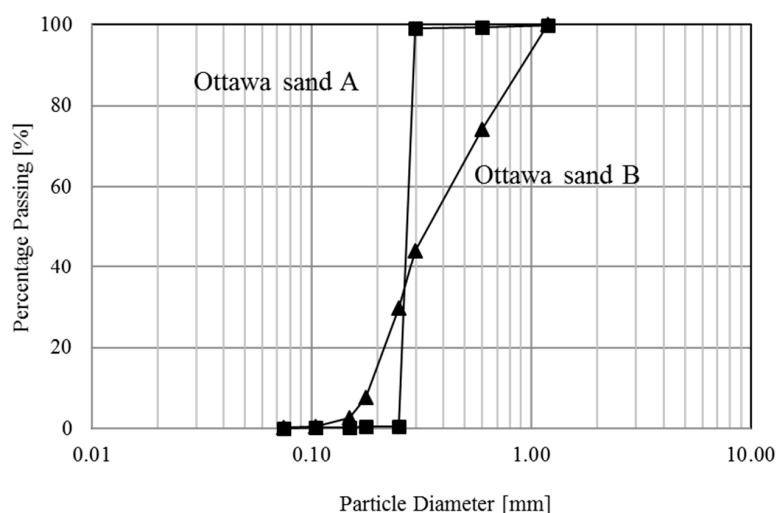


**Figure 2.** Particle size distributions of Ottawa sands.

**Table 1.** Particle size of the Ottawa sands in this study.

	Ottawa Sand A	Ottawa Sand A
* $D_{10}$	0.23	0.18
* $D_{50}$	0.25	0.32
* $C_u$	1.22	2.28
* $C_c$	0.86	0.72

\*  $D_{10}$  and  $D_{50}$  denote the grain diameters at 10% passing and 50% passing, respectively;  $C_u$ : coefficient of uniformity;  $C_c$ : coefficient of gradation.

### 3.2. Contact Angle

The sessile drop technique was employed to measure the contact angle of biopolymer solutions in decane (Figure 3). Pure silica plates (VWR VistaVision, Radnor, PA, USA—Cover Glasses, amorphous SiO<sub>2</sub>) were employed as the substrates that represent the silica sands, which were washed using ethanol (Mallinckrodt Baker, St. Louis, MO, USA, ACS reagent grade) prior to beginning each test. The silica plate was placed in a transparent chamber that was filled with decane. Biopolymer solution was introduced in the decane-filled chamber using a needle, and a droplet was foamed on a silica plate. The evolution of the biopolymer droplet was monitored using high-resolution time-lapse photography (Nikon D90, resolution: 12.3 megapixels). The obtained images were analysed using ImageJ (Bethesda, MD, USA) to measure the contact angle of the biopolymer solution. The test was repeated three times for each experimental condition and various biopolymer concentrations (i.e., 0, 2, 5 and 10 g/L).

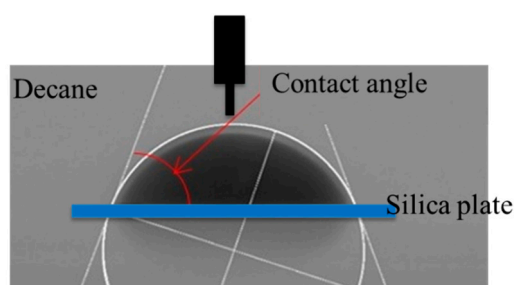


**Figure 3.** Experimental setup for contact angle measurement on silica surface submerged in decane.

### 3.3. Interfacial Tension

The Du Nouy ring method was employed to measure the interfacial tension between biopolymer solution and decane with a force Tensiometre (Sigma 703D). The container was half-filled with biopolymer solution. A platinum ring with a 6 cm diameter was submerged in biopolymer solution. Decane was introduced into the half-filled container with biopolymer solution, which was placed on the biopolymer solution due to its low density. While the platinum ring in the biopolymer solution was raised to enable the decane phase to form a fluid meniscus, the variation of forces was measured using a force tensiometer. The maximum force was measured when the meniscus in the platinum ring was torn, which was considered to be the interfacial tension between biopolymer solution and decane. The test was repeated three times for each experimental condition and various biopolymer concentrations (i.e., 0, 2, 5, and 10 g/L).

### 3.4. Viscosity

The viscosity of the biopolymer solutions was measured using a Brookfield Viscometer DV-III (Brookfield, Middleboro, MA, USA). A spindle, which rotated at a constant rate ( $3.4 \text{ s}^{-1}$ ), was immersed in the biopolymer solutions. The torque was measured while rotating the spindle at a constant rate and was analysed for the viscosity of fluids. A constant temperature was maintained at room temperature

(24 °C). The test was repeated three times for each experimental condition at various biopolymer concentrations (i.e., 0, 2, 5, and 10 g/L).

### 3.5. Biopolymer Solution-Decane Displacement

Figure 4 shows the experimental setup for biopolymer-decane displacement in oil-contaminated soils remediation tests. The wetting method was employed to prepare for the decane-saturated sands. One fifth of the soil chamber (inner diameter, ID, = 6.0 cm and height = 18.0 cm) was filled with decane, and dry sand was placed in the decane. This process was repeated five times to prepare for decane-saturated sand. The initial porosity of the sample was 0.381, which was applied to all tests. A small tubing chamber was placed between the transparent soil chamber and the syringe pump, which was filled with biopolymer (PEO and SA) solution and decane. Decane was always placed at the upper layer in the tubing chamber, as its density is lower than the density of the biopolymer solution. Although the syringe pump maintained constant flow rates of 10, 100, 200, 500, and 1000 mL/min, decane was injected into decane-saturated sand, and biopolymer solution was displaced with decane in the soil chamber. Injection of biopolymer solution was continued until biopolymer solution had percolated the decane-saturated sand. An additional twenty pore volumes (PV) of biopolymer solution were eventually injected into the decane-saturated sand after the biopolymer solution had percolated through the sand. Another small tubing chamber was connected to the outlet of the soil chamber, which recorded the amount of both biopolymer solution and decane that flowed out of the soil chamber and was used to estimate the biopolymer solution-decane displacement ratio. A constant room temperature of 24 °C was maintained.

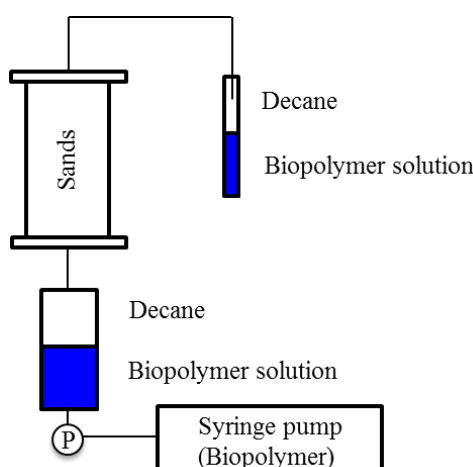


**Figure 4.** Experimental setup for decane-biopolymer displacement.

## 4. Results and Discussion

Experimental results obtained in this study are following. Analysis of variance (ANOVA) and student *t*-test methods were used for statistical analysis of data.

### 4.1. Contact Angle

Figure 5 shows the contact angles of biopolymer solution (PEO and SA) on the silica surface submerged in decane, which were measured for a variety of biopolymer concentrations (i.e., 0, 2, 5, and 10 g/L). Table 2 lists all measured contact angles, the mean values, and standard deviation, and Table 3 lists the *p* values by ANOVA and *t*-test. The results indicate that (1) the measured contact angles have less than 0.97° standard deviation; (2) the contact angles of the PEO and SA solutions, within the range of 0–10 g/L concentrations, are higher than the contact angles at atmospheric conditions. The contact angles of biopolymer solutions with 10 g/L PEO and 20 g/L SA are 37.2° at atmosphere and 41.2° at

atmosphere, respectively [8]. The results imply that the increased biopolymer contact angle on the silica plate submerged in decane can cause a decrease in the capillary entry pressure that is defined as a minimum required pressure to inject the PEO and SA solutions into oil-contaminated soil; (3) the contact angle of SA decreases with a maximum concentration of 2 g/L from 96.0° to 90.6° and remains relatively constant between 90.6° and 91.8°, within the range of 2–10 g/L. Note that the *p* values at 2 g/L to 5 g/L and 5 g/L to 10 g/L are 0.225 and 0.188, respectively (Table 3); (4) the contact angles of the PEO solution at 2–5 g/L concentrations (87.4°~92.2°) are lower than the contact angles of deionized water (96.0° ± 0.59°), while the contact angle of 10 g/L PEO solution (101.4° ± 0.59°) is higher than deionized water.

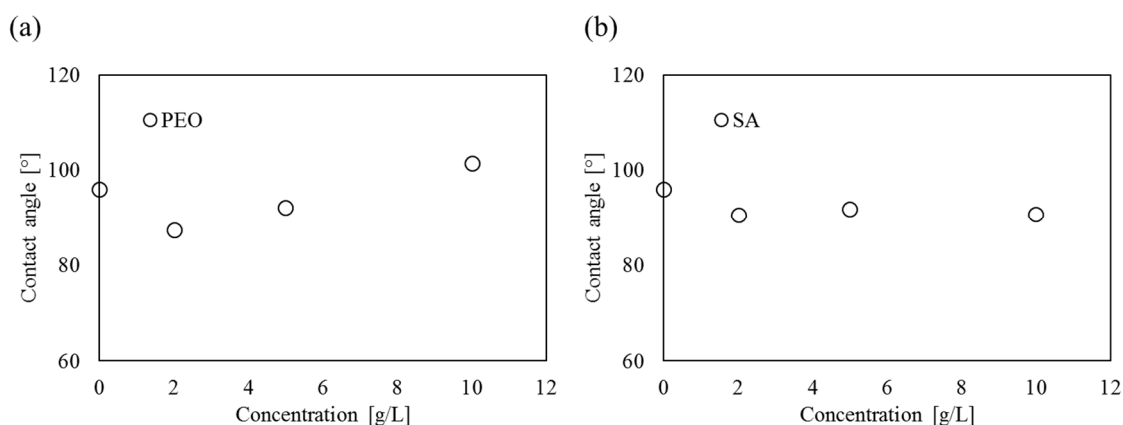


**Figure 5.** Contact angle variations according to the concentration changes of biopolymer solution: (a) PEO and (b) SA.

**Table 2.** Contact angle variations according to the concentration changes of biopolymer solution.

Concentration (g/L)	PEO			SA		
	Contact Angle (°)	Mean	Standard Deviation	Contact Angle (°)	Mean	Standard Deviation
0	95.2	96.0	0.59	95.2	96.0	0.59
	96.6					
	96.2					
2	87.2	87.4	0.17	90.1	90.6	0.68
	87.6					
	87.5					
5	92.2	92.2	0.16	91.2	91.8	0.97
	92.0					
	92.4					
10	100.8	101.4	0.59	90.3	90.7	0.39
	102.2					
	101.2					

PEO: polyethylene oxide; SA: sodium alginate.

**Table 3.** *p* values of contact angle by ANOVA and *t*-test.

Biopolymer Types	<i>p</i> Value			
	ANOVA		<i>t</i> -Test	
	0 g/L~10 g/L	0 g/L~2 g/L	2 g/L~5 g/L	5 g/L~10 g/L
PEO	$6.21 \times 10^{-9}$	$3.86 \times 10^{-5}$	$8.89 \times 10^{-6}$	$2.87 \times 10^{-5}$
SA	$1.51 \times 10^{-4}$	$1.10 \times 10^{-3}$	0.225	0.188

#### 4.2. Interfacial Tension

Figure 6 shows the results of the interfacial tension between the biopolymer solution (PEO and SA) and decane. Table 4 lists the measured interfacial tension, the mean values and the

standard deviation, and Table 5 lists the  $p$  values by ANOVA and  $t$ -test. The results indicate that (1) the water-decane interfacial tension ( $51.2 \pm 0.21$  mN/m) is lower than the water surface tension (72 mN/m); (2) biopolymer solution (PEO or SA)-decane interfacial tension is lower than the water-decane interfacial tension, which implies that the decreased interfacial tension influences the decrease in the capillary entry pressure to inject the biopolymer solution into the oil-contaminated soil; (3) the SA-decane interfacial tension is higher than the PEO-decane interfacial tension at the same concentration; (4) the interfacial tensions between the PEO solution and decane decreases up to 2 g/L concentration from  $51.2 \pm 0.21$  mN/m to  $26.0 \pm 0.16$  mN/m and then remains relatively constant within the 2–10 g/L concentration range (25.0~26.0 mN/m). Note that the  $p$  value at 2 g/L to 5 g/L and 5 g/L to 10 g/L is 0.06 (Table 5); (5) the interfacial tensions between the SA solution and decane also decrease up to 2 g/L concentration, from  $51.2 \pm 0.21$  mN/m to  $34.7 \pm 0.41$  mN/m, and then remain between  $34.7 \pm 0.41$  mN/m and  $39.5 \pm 0.33$  mN/m, within the 2–10 g/L concentration range.

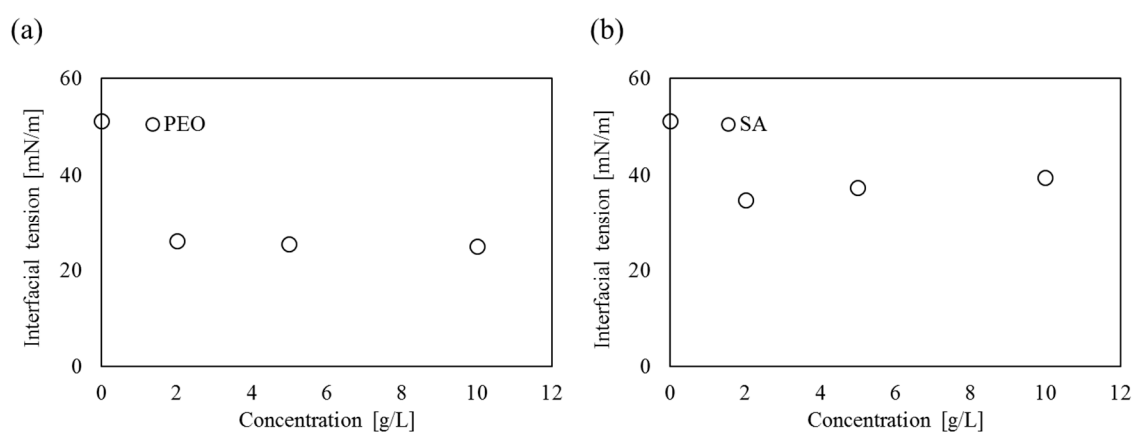


**Figure 6.** PEO-biopolymer solution interfacial tension variations according to the concentration changes of biopolymer solution: (a) PEO and (b) SA.

**Table 4.** Interfacial tension variations according to the concentration changes of biopolymer solution.

Concentration (g/L)	PEO			SA		
	Interfacial Tension (mN/m)	Mean	Standard Deviation	Interfacial Tension (mN/m)	Mean	Standard Deviation
0	51.2	51.2	0.21	51.2	51.2	0.21
	51.0			51.0		
	51.5			51.5		
2	26.2	26.0	0.16	34.2	34.7	0.41
	26.0			34.8		
	25.8			35.2		
5	25.8	25.5	0.25	37.2	37.4	0.16
	25.4			37.4		
	25.2			37.6		
10	25.1	25.0	0.12	39.5	39.5	0.33
	25.0			39.1		
	24.8			39.5		

**Table 5.**  $p$  values of interfacial tension by ANOVA and  $t$ -test.

Biopolymer Types	$p$ -Value			
	ANOVA	$t$ -Test		
	0 g/L~10 g/L	0 g/L~2 g/L	2 g/L~5 g/L	5 g/L~10 g/L
PEO	$1.85 \times 10^{-14}$	$1.76 \times 10^{-8}$	0.06	0.06
SA	$5.38 \times 10^{-11}$	$9.00 \times 10^{-7}$	$1.03 \times 10^{-3}$	$1.24 \times 10^{-3}$

### 4.3. Viscosity

Figure 7 shows the results of the viscosities of the biopolymer (PEO and SA) solutions, with respect to their concentrations for a variety of shear rates ( $1\text{--}10\text{ s}^{-1}$ ). The results indicate that (1) the viscosity of PEO and SA is higher than the viscosity of DI water. Compared with other biopolymers in the literature review, the viscosity in this study ( $1.523 \times 10^{-3}\text{--}1.867 \times 10^{-3}\text{ Pa}\cdot\text{s}$ ) is higher, at the same concentration (2 g/L) and shear rates ( $1\text{--}10\text{ s}^{-1}$ ), than chitosan ( $7.76 \times 10^{-4}\text{--}2.415 \times 10^{-3}\text{ Pa}\cdot\text{s}$ ) but is lower than the viscosities of Xanthan gum ( $0.0665\text{--}0.168\text{ Pa}\cdot\text{s}$ ) and polyacrylic acid (PAA) ( $0.126\text{--}0.408\text{ Pa}\cdot\text{s}$ ) [8]; (2) the viscosity increases with an increase in the biopolymer solution concentration, within the range of  $0\text{--}10\text{ g/L}$  (Figure 7); (3) the viscosity decreases with increased shear rates, from  $1\text{ s}^{-1}$  to  $10\text{ s}^{-1}$  (Figure 8), which is consistent with the previous study [7]. Jung et al. (2016) presented that the viscosities of the biopolymer solutions decrease with an increase in the shear rate between  $3.4\text{ s}^{-1}$  and  $17\text{ s}^{-1}$  [7]. At a given biopolymer concentration ( $0\text{--}10\text{ g/L}$ ) and shear rate ( $1\text{--}10\text{ s}^{-1}$ ), the viscosity change of PEO and SA by the increased concentration of PEO (or SA) is more prominent than the viscosity change of PEO and SA by the decreased shear rate. For example, the viscosity of the PEO solution changed from  $0.00185\text{ Pa}\cdot\text{s}$  to  $0.0153\text{ Pa}\cdot\text{s}$  at  $1\text{ s}^{-1}$ , with an increased concentration from 0 to  $10\text{ g/L}$ . However the viscosity of the PEO solution changed from  $1.85 \times 10^{-3}\text{ Pa}\cdot\text{s}$  to  $9.81 \times 10^{-4}\text{ Pa}\cdot\text{s}$  at  $0\text{ g/L}$  concentration with an increase in shear rates from 1 to  $10\text{ s}^{-1}$ .

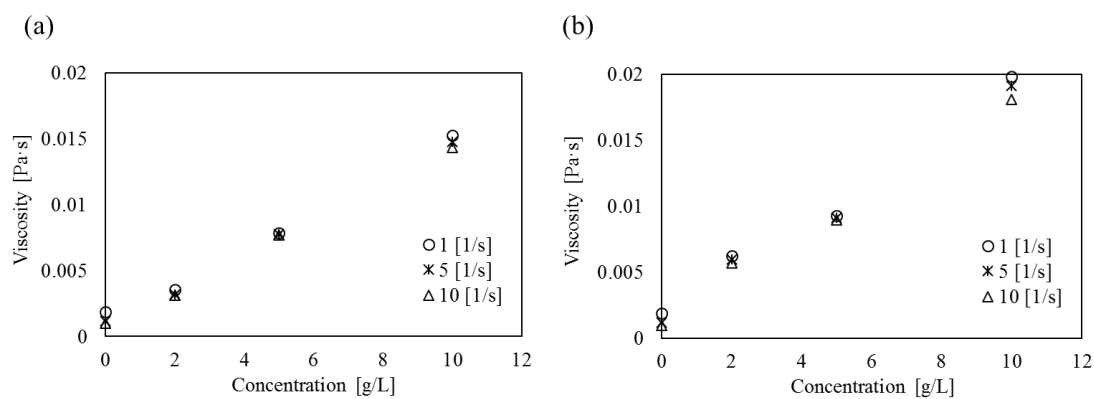


**Figure 7.** Viscosity variations according to the concentration changes of biopolymer solution: (a) PEO and (b) SA.

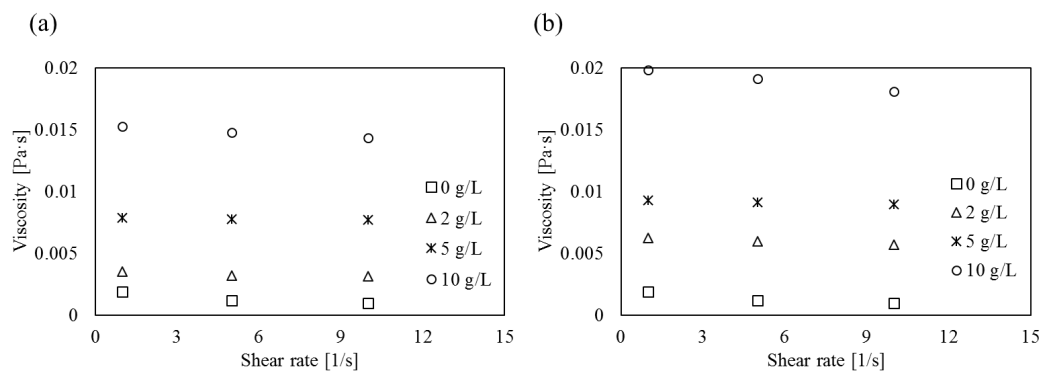


**Figure 8.** Viscosity variations according to the shear rate changes of biopolymer solution: (a) PEO and (b) SA.

### 4.4. Biopolymer Solution-Decane Displacement

Figure 9 shows the values of the biopolymer solution-decane displacement ratios with respect to the biopolymer injection flow rate into decane-saturated soils. The results indicate that (1) the

biopolymer solution-decane displacement ratio increases with respect to the concentration of the biopolymer at the same flow rate. A solution with a high viscosity at a high biopolymer concentration causes the displacement ratio to increase; (2) the displacement ratio of both the PAM solution and the SA solution consistently increases with an increase in the values of the flow rate. The effect of the flow rate is more prominent for a low biopolymer concentration. High concentrations (>10 g/L of PAM or >5 g/L of SA) show fewer effects of flow rate on the displacement ratio. For example, when PEO solution concentration is 10 g/L, the displacement ratio increases from 89% to 91%, with an increase of flow rate from 10 mL/min to 1000 mL/min.

Results imply that biopolymer concentration governs the displacement ratio in low flow rates (i.e., 10 mL/min in this study). However the rapid flow rate governs the displacement ratio instead of viscosity. Thus soil remediation would be cost-effective at high flow rates but with moderate biopolymer concentration levels (i.e., faster than 100 mL/L at 2 to 5 g/L of PAM or SA).

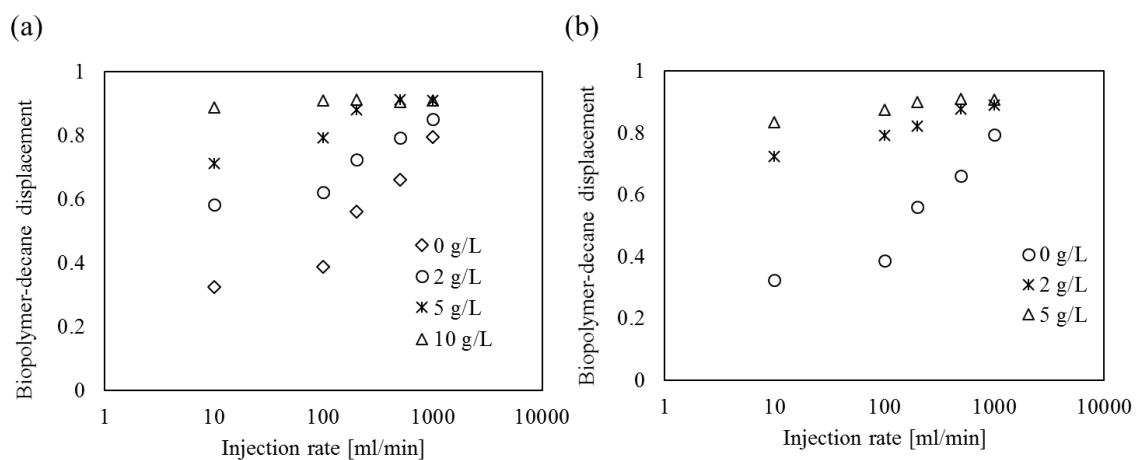


**Figure 9.** Biopolymer solution-decane displacement according to the increase in injection rate, (a) PEO; (b) SA.

#### 4.5. Displacement Ratios as a Function of Viscous Number ( $N_m$ ) and Capillary Number ( $N_c$ )

When a fluid is injected into other, fluid-saturated, porous media, the fluid invasion pattern is inherently governed by the following two dimensionless numbers [55,56];

$$N_m = \frac{\mu_{inv}}{\mu_{def}} \quad (1)$$

$$N_c = \frac{\mu_{inv} v}{\sigma \cdot \cos\theta} \quad (2)$$

where  $N_m$  is the viscous number that is defined as the ratio of the injected fluid viscosity  $\mu_{inv}$  and the defensed fluid viscosity  $\mu_{def}$ .  $N_c$  is the capillary number that represents the ratio of the viscous force over the capillary force, which is associated with the injected fluid velocity  $v_{inv}$ , the injected fluid viscosity  $\mu_{inv}$ , the contact angle  $\theta$ , and the interfacial tension  $\sigma$ . These two dimensionless numbers ( $N_m$  and  $N_c$ ) govern three dominant regions with distinct invasion patterns and efficiencies (Figure 10); capillary fingering, viscous fingering, and stable displacement [57,58]. Figure 10 shows three dominant regions with  $N_m$  and  $N_c$  values for each test in this study; these values are calculated according to Equations (1) and (2), respectively. The biopolymer solution injecting velocity  $v_{inv}$  is calculated as the injection flow velocity divided by the average cross-sectional pore area of the sample, which is calculated as the pore volume divided by the length of the sample. For example, the injection rate of 100 mL/min corresponds to the injection velocity of 9.28 cm/min. Figure 10 also includes the  $N_m$  and  $N_c$  values in our experiments, which are located in the transition region among the invading patterns represented by Lenormand [55]. The shape and colour of the data are equivalent to the

concentration of PEO or SA in Figure 10, which cause the variation in  $N_c$  at the constant  $N_m$ , due to the change in injection rate. Within this region, the biopolymer solution-decane displacement ratio clearly increases with  $N_c$  (Figure 11). However distinct relations between the displacement ratio and  $N_m$  were not observed. This finding is conceptually consistent with the previous pore network simulation results [59] and previous experimental studies [8]. Thus an increase in the  $N_c$  value is required to increase the biopolymer-decane displacement ratio. As  $N_c$  is proportional to the injecting velocity  $v_{inv}$ , the injected biopolymer viscosity  $\mu_{inv}$ , and the contact angle on the mineral surface  $\theta$ , but inversely proportional to the interfacial tension  $\sigma$  (Equation (2)), the following recommendations may increase the biopolymer-decane displacement ratio; (1) increase the biopolymer injection velocity, and (2) increase the biopolymer solution viscosity with a high concentration of biopolymer solutions.

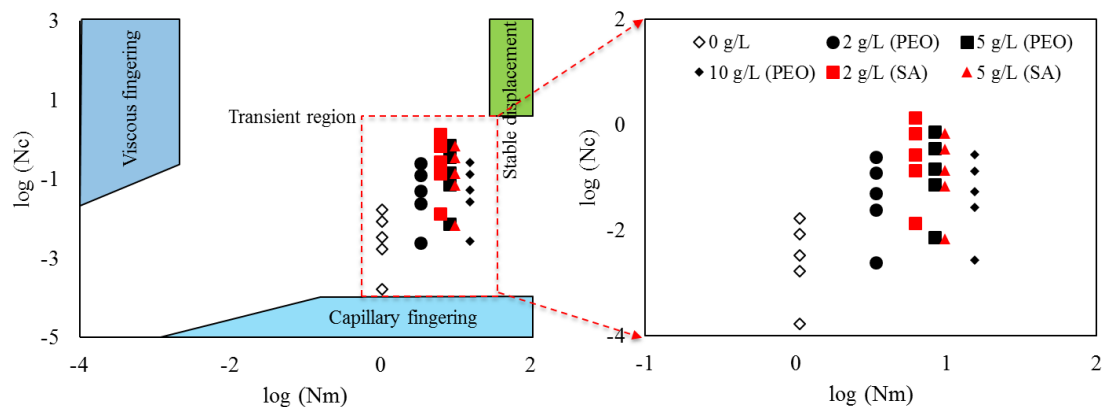


Figure 10. Viscous number ( $N_m$ ) and capillary number ( $N_c$ ).

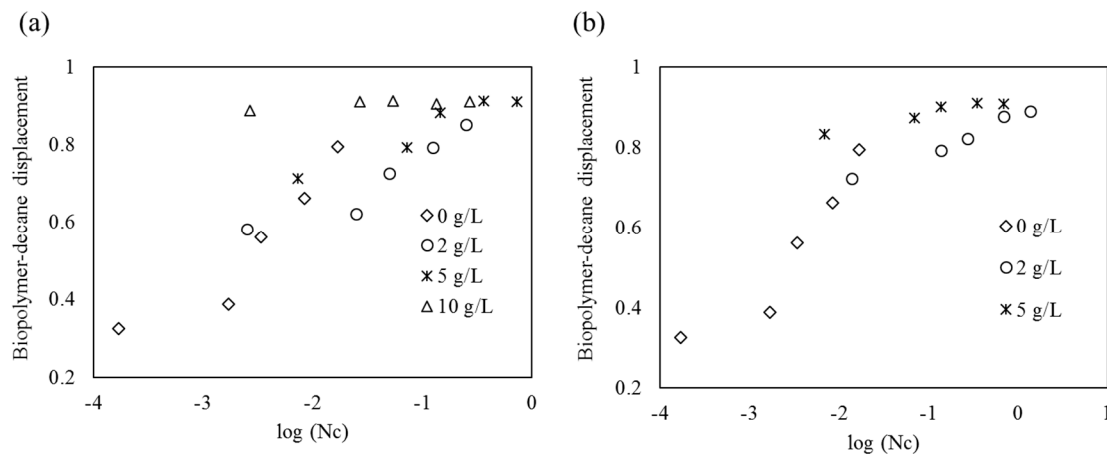
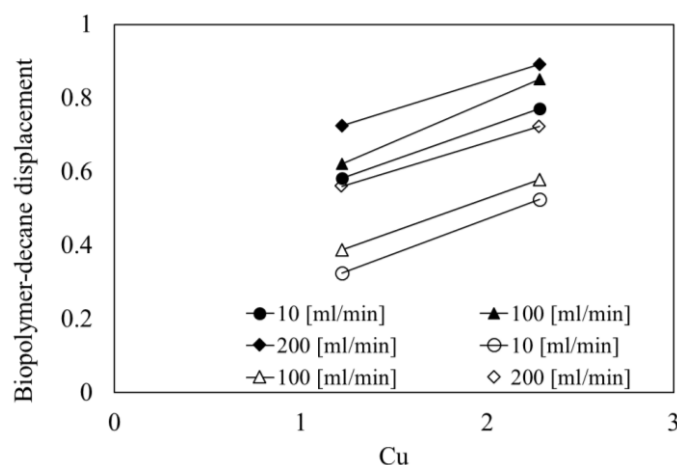


Figure 11. Biopolymer solution-decane displacement according to the change in capillary number  $\log(N_c)$ , (a) PEO; (b) SA.

#### 4.6. Effect of Particle Size Distribution on Biopolymer-Decane Displacement

Two samples with different particle size distributions (Figure 2) were employed in this study. Table 1 lists information about the particles. Although both samples have poorly graded particle size distributions, they reveal the distinct differences in distribution. Figure 12 shows the biopolymer-decane displacement ratio with the change in the coefficient of uniformity  $C_u$ . The biopolymer-decane displacement ratio increases with an increase in the coefficient of uniformity  $C_u$ , within the range of flow rates from 10 to 200 mL/min. This result implies that extensively distributed particle sizes hinder the fingering, which induces a high biopolymer-decane displacement ratio at the same flow rate.



**Figure 12.** Biopolymer solution-decane displacement at the change in the coefficient of uniformity  $C_u$ .

## 5. Conclusions

The biopolymer solutions PEO and SA are tested to identify the effect of the biopolymer concentration on contact angle, interfacial tension, and viscosity. Oil-contaminated soil remediation tests have been conducted using two soil samples with distinctly different particle size distributions. The contact angles of PEO and SA solutions are higher than the contact angles at atmospheric conditions. The biopolymer solution (PEO or SA)-decane interfacial tension is lower than the water-decane interfacial tension, and a relatively small change was observed within the given range of concentration (2–10 g/L). Thus the increased contact angle and decreased interfacial tension cause the capillary entry pressure to decrease. The viscosities of PEO and SA are higher than the viscosities of deionized (DI) water and increase with concentration, which causes the biopolymer solution-decane displacement ratio to increase. The biopolymer solution-decane displacement ratio increases with the injection rate (the maximum rate validated in this study was 92.8 cm/min). This trend was applied to various concentrations of PAM and SA (i.e., 2, 5, and 10 g/L of PAM and SA solutions). High concentrations of PAM and SA increase the total displacement ratio due to the increase in viscosity with concentration. At a low injection rate, the effect of the concentration of PEO and SA on displacement is more prominent. However the effect of concentration is minimal due to an increase in injection velocity. The biopolymer solution-decane displacement ratio increases with the capillary number  $N_c$  due to the increased flow rate. Thus the factors (i.e., injection rate, biopolymer viscosity, contact angle and interfacial tension) in Equation (2) should be controlled to increase the remediation efficiency. Both injection rate and viscosity show significant effects on soil remediation efficiency in this study. The biopolymer-decane displacement ratio increases with an increase in the coefficient of uniformity  $C_u$ , within the range of flow rates from 10 to 200 mL/min.

**Author Contributions:** Jongwon Jung and Jong Wan Hu conceived and designed the experiments; Jongwon Jung performed the experiments; and Jong Wan Hu analysed the data and wrote the paper. All authors read and approved the final manuscript.

**Conflicts of Interest:** The authors declare no conflict of interest.

## References

1. Mitchell, R.; Nevo, Z. Effect of bacterial polysaccharide accumulation on infiltration of water through sand. *Appl. Microbiol. Biotechnol.* **1964**, *12*, 219–223.
2. Bate, B.; Zhao, Q.; Burns, S. Impact of organic coatings on frictional strength of organically modified clay. *J. Geotechn. Geoenviron. Eng.* **2013**, *140*, 228–236. [CrossRef]
3. Briscoe, W.H.; Klein, J. Friction and adhesion hysteresis between surfactant monolayers in water. *J. Adhes.* **2007**, *83*, 705–722. [CrossRef]

4. Cabalar, A.; Canakci, H. *Ground Improvement by Bacteria*; Taylor and Francis Group: Abingdon, UK, 2005.
5. Kang, X.; Kang, G.C.; Bate, B. Shear wave velocity anisotropy of kaolinite using a floating wall consolidometer-type bender element testing system. *Geotech. Test. J.* **2014**, *37*, 1–15. [[CrossRef](#)]
6. Kavazanjian, E., Jr.; Iglesias, E.; Karatas, I. Biopolymer soil stabilization for wind erosion control. In Proceedings of the 17th International Conference on Soil Mechanics and Geotechnical Engineering, Alexandria, Egypt, 5–9 October 2009; pp. 881–884.
7. Jung, J.; Jang, J.; Ahn, J. Characterization of a polyacrylamide solution used for remediation of petroleum contaminated soils. *Materials* **2016**, *9*, 16. [[CrossRef](#)]
8. Cao, S.C.; Bate, B.; Hu, J.W.; Jung, J. Engineering behavior and characteristics of water-soluble polymers: Implication on soil remediation and enhanced oil recovery. *Sustainability* **2016**, *8*, 205. [[CrossRef](#)]
9. Sojka, R.E.; Bjorneberg, D.L.; Entry, J.A.; Lentz, R.D.; Orts, W.J. Polyacrylamide in agriculture and environmental land management. *Adv. Agron.* **2007**, *92*, 75–162.
10. Jung, J.; Jang, J. Soil-water characteristic curve of sediments containing a polyacrylamide solution. *Geotech. Lett.* **2016**, *1*, 1–6. [[CrossRef](#)]
11. Inbar, A.; Ben-Hur, M.; Sternberg, M.; Lado, M. Using polyacrylamide to mitigate post-fire soil erosion. *Geoderma* **2015**, *239–240*, 107–114. [[CrossRef](#)]
12. Lentz, R.D. Polyacrylamide and biopolymer effects on flocculation, aggregate stability, and water seepage in a silt loam. *Geoderma* **2015**, *241–242*, 289–294. [[CrossRef](#)]
13. Lee, S.S.; Shah, H.S.; Awad, Y.M.; Kumar, S.; Ok, Y.S. Synergy effects of biochar and polyacrylamide on plants growth and soil erosion control. *Environ. Earth Sci.* **2015**, *74*, 1–11. [[CrossRef](#)]
14. Hove, A.O.; Nilson, V.; Loknes, J. Visualization of xanthan flood behavior in core samples by means of X-ray tomography. *SPE Reserv. Eng.* **1990**, *5*, 475–480. [[CrossRef](#)]
15. Philips, J.C.; Miller, J.W.; Wernau, W.C.; Tate, B.E.; Auerbach, M.H. A high-pyruvate xanthan for EOR. *Soc. Pet. Eng. J.* **1985**, *25*, 594–602. [[CrossRef](#)]
16. Pollock, T.J.; Thorne, L. Xanthomonas Campestris Strain for Production of Xanthan Gum. U.S. Patent 5,279,961 A, 18 January 1994.
17. Sandiford, B.B. Laboratory and field studies of water floods using polymer solutions to increase oil recoveries. *J. Pet. Technol.* **1964**, *16*, 917–922. [[CrossRef](#)]
18. Strom, T.E.; Paul, J.M.; Phelps, C.H.; Sampath, K. A new biopolymer for high-temperature profile control: Part 1-laboratory testing. *Soc. Pet. Eng. J.* **1991**, *6*, 360–364. [[CrossRef](#)]
19. Blokker, N.C.M. Analysis of alginate-like exopolysaccharides for the application in enhanced oil recovery. Master's Thesis, Delft University of Technology, Delft, The Netherlands, 2014.
20. Bailey, S.A.; Bryant, R.S.; Duncan, K.E. *Use of Biocatalysts for Triggering Biopolymer Gelants*; Society of Petroleum Engineers: Tulsa, OK, USA, 2000.
21. Kosaric, N. Biosurfactants and their application for soil bioremediation. *Food Technol. Biotechnol.* **2001**, *39*, 295–304.
22. Leveratto, M.A.; Lauri, J.; Sanz, C.; Sigal, J.; Farouq Ali, S.M. EOR polymer screening for an oil field with high salinity brines. *Soc. Pet. Eng. J.* **1996**, *4*, 73–81. [[CrossRef](#)]
23. Kahovec, J.; Fox, R.B.; Hatada, K. Nomenclature of regular single-strand organic polymers. *Pure Appl. Chem.* **2002**, *74*, 1921–1956. [[CrossRef](#)]
24. Martin, G.; Yen, T.; Karimi, S. In Application of biopolymer technology in silty soil matrices to form impervious barriers. In Proceedings of the 7th Australia-New Zealand Geomechanics Conference, Adelaide, Australia, 1–5 July 1996.
25. Meuser, H. *Soil Remediation and Rehabilitation*; Springer: Dordrech, The Netherlands, 2010; Volume 23, pp. 1–2.
26. Daripa, P.; Paşa, G. On capillary slowdown of viscous fingering in immiscible displacement in porous media. *Transp. Porous Med.* **2008**, *75*, 1–16. [[CrossRef](#)]
27. Mulligan, C.N. Environmental applications for biosurfactants. *Environ. Pollut.* **2005**, *133*, 183–198. [[CrossRef](#)] [[PubMed](#)]
28. Chai, J.-C.; Miura, N. Field vapor extraction test and long-term monitoring at a PCE contaminated site. *J. Hazard. Mater.* **2004**, *110*, 85–92. [[CrossRef](#)] [[PubMed](#)]
29. Cho, J.S.; Wilson, J.T.; DiGiulio, D.C.; Vardy, J.A.; Choi, W. Implementation of natural attenuation at a JP-4 jet fuel release after active remediation. *Biodegradation* **1997**, *8*, 265–273. [[CrossRef](#)] [[PubMed](#)]

30. Tse, K.K.; Lo, S.-L.; Wang, J.W. Pilot study of in-situ thermal treatment for the remediation of pentachlorophenol-contaminated aquifers. *Environ. Sci. Technol.* **2001**, *35*, 4910–4915. [[CrossRef](#)] [[PubMed](#)]
31. Mulligan, C.N.; Eftekhari, F. Remediation with surfactant foam of PCP-contaminated soil. *Eng. Geol.* **2003**, *70*, 269–279. [[CrossRef](#)]
32. Knox, R.C.; Sabatini, D.A. *Transport and Remediation of Subsurface Contaminants*; American Chemical Society: Washington, DC, USA, 1992.
33. Lee, M.; Kim, J.; Kim, I. In-situ biosurfactant flushing, coupled with a highly pressurized air injection, to remediate the bunker oil contaminated site. *Geosci. J.* **2011**, *15*, 313–321. [[CrossRef](#)]
34. Khatami, H.R.; O’Kelly, B.C. Improving mechanical properties of sand using biopolymers. *J. Geotech. Geoenviron. Eng.* **2012**, *139*, 1402–1406. [[CrossRef](#)]
35. Chang, I.; Cho, G.-C. Strengthening of Korean residual soil with  $\beta$ -1,3/1,6-glucan biopolymer. *Constr. Build. Mater.* **2012**, *30*, 30–35. [[CrossRef](#)]
36. Chang, I.; Im, J.; Prasadhi, A.K.; Cho, G.-C. Effect of Xanthan gum biopolymer on soil strengthening. *Constr. Build. Mater.* **2015**, *74*, 65–72. [[CrossRef](#)]
37. Jafvert, C.T. *Surfactants/Cosolvents*; Ground-Water Remediation Technologies Analysis Center: Pittsburgh, PA, USA, 1996.
38. Jawitz, J.W.; Annable, M.D.; Rao, P. Miscible fluid displacement stability in unconfined porous media: Two-dimensional flow experiments and simulations. *J. Contam. Hydrol.* **1998**, *31*, 211–230. [[CrossRef](#)]
39. Lee, M.; Kang, H.; Do, W. Application of nonionic surfactant-enhanced in situ flushing to a diesel contaminated site. *Water Res.* **2005**, *39*, 139–146. [[CrossRef](#)] [[PubMed](#)]
40. Mulligan, C.; Yong, R.; Gibbs, B. Remediation technologies for metal-contaminated soils and groundwater: An evaluation. *Eng. Geol.* **2001**, *60*, 193–207. [[CrossRef](#)]
41. Park, J.-Y.; Kim, S.-J.; Lee, Y.-J.; Baek, K.; Yang, J.-W. Ek-fenton process for removal of phenanthrene in a two-dimensional soil system. *Eng. Geol.* **2005**, *77*, 217–224. [[CrossRef](#)]
42. Tsai, T.-T.; Kao, C.-M.; Yeh, T.-Y.; Liang, S.-H.; Chien, H.-Y. Remediation of fuel oil-contaminated soils by a three-stage treatment system. *Environ. Eng. Sci.* **2009**, *26*, 651–659. [[CrossRef](#)]
43. Zhou, W.; Fu, H.; Pan, K.; Tian, C.; Qu, Y.; Lu, P.; Sun, C.-C. Mesoporous  $\text{TiO}_2/\alpha\text{-Fe}_2\text{O}_3$ : Bifunctional composites for effective elimination of arsenite contamination through simultaneous photocatalytic oxidation and adsorption. *J. Phys. Chem. C* **2008**, *112*, 19584–19589. [[CrossRef](#)]
44. Sorbie, K. Introduction to polymer flooding. In *Polymer-Improved Oil Recovery*; Springer: Dordrech, The Netherlands, 1991; pp. 1–5.
45. Kim, P.; Wong, T.S.; Alvarenga, J.; Kreder, M.J.; Adorno-Martinez, W.E.; Aizenberg, J. Liquid-infused nanostructured surfaces with extreme anti-ice and anti-frost performance. *ACS Nano* **2012**, *6*, 6569–6577. [[CrossRef](#)] [[PubMed](#)]
46. Bruun, J.; Hicks-Bruun, M. Isolation of n-decane from petroleum by distillation and equilibrium melting. *J. Res. Natl. Bur. Stand.* **1932**, *8*, 583–589. [[CrossRef](#)]
47. Fan, R.; Guo, S.; Li, T.; Li, F.; Yang, X.; Wu, B. Contributions of electrokinetics and bioremediation in the treatment of different petroleum components. *Clean Soil Air Water* **2015**, *43*, 251–259. [[CrossRef](#)]
48. Fu, W.J.; Chi, Z.; Ma, Z.C.; Zhou, H.X.; Liu, G.L.; Lee, C.F.; Chi, Z.M. Hydrocarbons, the advanced biofuels produced by different organisms, the evidence that alkanes in petroleum can be renewable. *Appl. Microbiol. Biotechnol.* **2015**, *99*, 7481–7494. [[CrossRef](#)] [[PubMed](#)]
49. Margesin, R.; Moertelmaier, C.; Mair, J. Low-temperature biodegradation of petroleum hydrocarbons (n-alkanes, phenol, anthracene, pyrene) by four actinobacterial strains. *Int. Biodeterior. Biodegrad.* **2013**, *84*, 185–191. [[CrossRef](#)]
50. Bertrand, E.M.; Keddis, R.; Groves, J.T.; Vetriani, C.; Austin, R.N. Identity and mechanisms of alkane-oxidizing metalloenzymes from deep-sea hydrothermal vents. *Front. Microbiol.* **2013**, *4*, 109. [[CrossRef](#)] [[PubMed](#)]
51. Zemo, D.A.; Bruya, J.E.; Graf, T.E. The application of petroleum hydrocarbon fingerprint characterization in site investigation and remediation. *Ground Water Monit. Remediat.* **1995**, *15*, 147–156. [[CrossRef](#)]
52. Rayner, J.L.; Snape, I.; Walworth, J.L.; Harvey, P.M.; Ferguson, S.H. Petroleum-hydrocarbon contamination and remediation by microbioventing at sub-antarctic macquarie island. *Cold Reg. Sci. Technol.* **2007**, *48*, 139–153. [[CrossRef](#)]

53. Nadim, F.; Hoag, G.E.; Liu, S.; Carley, R.J.; Zack, P. Detection and remediation of soil and aquifer systems contaminated with petroleum products: An overview. *J. Pet. Sci. Eng.* **2000**, *26*, 169–178. [[CrossRef](#)]
54. Zyakun, A.; Nii-Annang, S.; Franke, G.; Fischer, T.; Buegger, F.; Dilly, O. Microbial activity and <sup>13</sup>C/<sup>12</sup>C ratio as evidence of N-hexadecane and N-hexadecanoic acid biodegradation in agricultural and forest soils. *Geomicrobiol. J.* **2012**, *29*, 570–584. [[CrossRef](#)]
55. Lenormand, R. Liquids in porous media. *J. Phys. Condens. Matter* **1990**, *2*, 79. [[CrossRef](#)]
56. Lenormand, R.; Touboul, E.; Zarcone, C. Numerical models and experiments on immiscible displacements in porous media. *J. Fluid Mech.* **1988**, *189*, 165–187. [[CrossRef](#)]
57. Lenormand, R.; Zarcone, C.; Sarr, A. Mechanisms of the displacement of one fluid by another in a network of capillary ducts. *J. Fluid Mech.* **1983**, *135*, 337–353. [[CrossRef](#)]
58. Buchgraber, M. *An Enhanced Oil Recovery Micromodel Study with Associative and Conventional Polymers*; University of Leoben: Leoben, Austria, 2008; pp. 16–30.
59. Ferer, M.; Bromhal, G.S.; Smith, D.H. Pore-level modeling of carbon dioxide sequestration in brine fields. *J. Energy Environ. Res.* **2002**, *2*, 120–132.



© 2017 by the authors; licensee MDPI, Basel, Switzerland. This article is an open access article distributed under the terms and conditions of the Creative Commons Attribution (CC-BY) license (<http://creativecommons.org/licenses/by/4.0/>).